Monthly Notices of the ROYAL ASTRONOMICAL SOCIETY

MNRAS **500,** 558–564 (2021) doi:10.1093/mnras/staa3216
Advance Access publication 2020 October 22

Double-peaked Lyman α emission at $z = 6.803$: a reionization-era galaxy self-ionizing its local H II bubble

Romain A. Meyer [1]★ Nicolas Laporte,[2,3] Richard S. Ellis,[1] Anne Verhamme[4,5] and Thibault Garel[4,5]

[1]*Department of Physics and Astronomy, University College London, Gower Street, London WC1E 6BT, UK*
[2]*Kavli Institute for Cosmology, University of Cambridge, Madingley Road, Cambridge CB3 0HA, UK*
[3]*Cavendish Laboratory, University of Cambridge, 19 JJ Thomson Avenue, Cambridge CB3 0HE, UK*
[4]*Observatoire de Geneve, Universite de Geneve, 51 Ch. des Maillettes, 1290 Versoix, Switzerland*
[5]*Univ. Lyon1, ENS de Lyon, CNRS, Centre de Recherche Astrophysique de Lyon UMR5574, F-69230, Saint-Genis-Laval, France*

Accepted 2020 October 12. Received 2020 October 12; in original form 2020 May 14

ABSTRACT

We report the discovery of a double-peaked Lyman α profile in a galaxy at $z = 6.803$, A370p_z1, in the parallel Frontier Field of Abell 370. The velocity separation between the blue and red peaks of the Lyman α profile ($\Delta v = 101^{+38}_{-19}(\pm 48)\,\mathrm{km\,s^{-1}}$) suggests an extremely high escape fraction of ionizing photons $> 59(51)$ per cent(2σ). The spectral energy distribution indicates a young (50 Myr), star-forming ($12 \pm 6\,\mathrm{M_{\odot}yr^{-1}}$) galaxy with an IRAC excess implying strong [O III] + H β emission. On the basis of the high escape fraction measured, we demonstrate that A370p_z1 was solely capable of creating an ionized bubble sufficiently large to account for the blue component of its Lyman α profile. We discuss whether A370p_z1 may be representative of a larger population of luminous $z \simeq 7$ double-peaked Lyman α emitting sources with high escape fractions that self-ionized their surroundings without contributions from associated ultraviolet-fainter sources.

Key words: galaxies: high-redshift – dark ages, reionization, first stars.

1 INTRODUCTION

Cosmic reionization marks the last phase transition of the Universe when the intergalactic medium (IGM) was reionized, thus ending the so-called dark ages. The timing of reionization is now constrained to $5.5 \lesssim z \lesssim 15$ by a variety of probes (Stark et al. 2010; Becker et al. 2015b; Planck Collaboration VI 2018; Bañados et al. 2019). Yet the sources capable of emitting sufficient ionizing photons by $z \sim 5.5$ continue to be the subject of debate (e.g. see sections 7 and 8 of Dayal & Ferrara 2018, for a review). A widely held view is that intrinsically ultraviolet (UV)-faint galaxies are the primary contributors, typically leaking ~ 10 per cent of their Lyman continuum (LyC) photons to the IGM (e.g. Robertson et al. 2015; Finkelstein et al. 2019; Dayal et al. 2020). However, to match the relative rapid decline of the neutral fraction at late times, rarer, luminous sources may play a significant role (e.g. Naidu et al. 2020). The issue remains unsolved as there is yet no direct way of measuring the escape fraction, $f_{\rm esc}$(LyC), of LyC radiation at high redshift.

At $z < 4$, LyC leakers are being studied in detail providing new insight into the physical conditions under which ionizing photons can escape. A picture is emerging where LyC leakage may be linked to the [O III]/[O II] emission line ratio (Nakajima et al. 2018, 2020, but see also Bassett et al. (2019)), varies geometrically due to low column density channels which allow the photons to escape (Fletcher et al. 2019) and is correlated with the Lyman α emission line profile (e.g. Verhamme et al. 2015; Izotov et al. 2018). Of particular interest is the correlation with the velocity separation in double-peaked Lyman α profiles (e.g. Izotov et al. 2018). As Lyman α photons are scattered and Doppler-shifted in dense neutral gas before emerging out of resonance on either the blue or red side of the peak, the double-peaked separation is linked to the H I column density that controls the LyC escape fraction (Verhamme et al. 2015; Kakiichi & Gronke 2019). Moreover, after the Lyman α photons escape, only a modest amount of neutral gas in the IGM would absorb the blue wing (Dijkstra 2014). Double-peaked Lyman α emitters thus also constrain the size of any associated ionized bubble (e.g. Mason & Gronke 2020).

Thus far, only two galaxies at $z > 6$ [NEPLA4, $z = 6.54$ (Songaila et al. 2018) and COLA1, $z = 6.59$ (Hu et al. 2016; Matthee et al. 2018)] are known to have a double-peaked Lyman α profile. Bosman et al. (2020) also recently reported a double-peaked profile in a $z \sim 5.8$ Lyman-Break selected galaxy, Aerith B, in the near-zone of a quasar. The peak velocity separation measured in the three Lyman α profiles have provided useful estimates of $f_{\rm esc}$(LyC) in high-redshift galaxies. In this paper, we report the discovery of a new galaxy presenting a double-peaked Lyman α profile at $z = 6.803$, deeper in the reionization era than those above. Its Lyman α profile indicates a much larger escape fraction and a capability to self-ionize its local H II bubble. We discuss whether it is representative of those sources that ended cosmic reionization. Throughout this paper, magnitudes are in the AB system (Oke 1974), and we use a concordance cosmology with $H_0 = 70$, $\Omega_{\rm M} = 0.3$, $\Omega_{\Lambda} = 0.7$. We refer to proper (comoving) kiloparsecs and megaparsecs as p(c)kpc and p(c)Mpc.

2 OBSERVATIONS

The target of this study was originally observed as part of a search for rest-frame UV lines signalling active galactic nucleus (AGN) activity in bright $z \sim 7$ galaxies [X-Shooter/VLT, ID: 0100.A-0664(A), PI: Laporte]. Following earlier detection of He II emission in a galaxy

★ E-mail: r.meyer.17@ucl.ac.uk, meyer@mpia.de

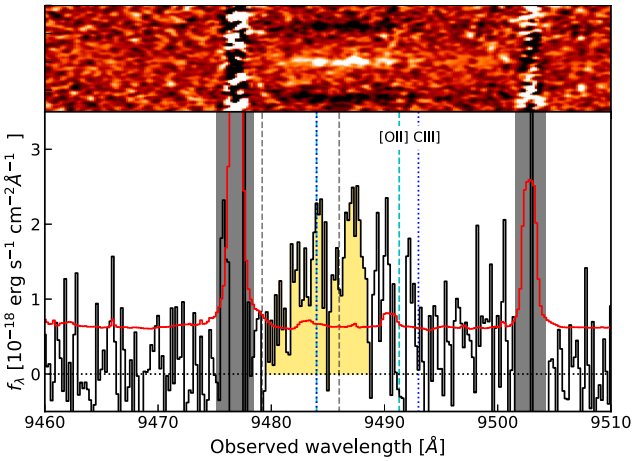

Figure 1. 2D spectra of A370p_z1, showing double-peaked Lyman α emission at $z = 6.803$ with two negative counterparts arising from the telescope dither pattern. The lower panel shows the 1D spectrum (black) and error array (red) with OH sky lines masked in grey. The two peaks are highlighted in yellow. Vertical dotted lines show the maximum extent of the blue wing and the mid-point of the two peaks. The velocity separation of emission line doublets of potential low-redshift redshift interlopers is illustrated by cyan dashed ([O II]$\lambda\lambda$3727, 3729) and blue dotted (C III]$\lambda\lambda$1907, 1909) vertical lines, with the first peak of the doublets placed at the observed blue peak wavelength $\lambda = 9484$ Å.

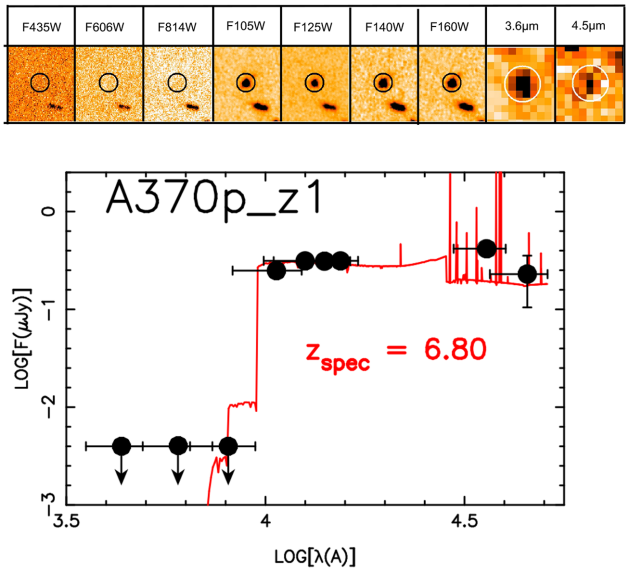

Figure 2. *Top panel*: Frontier field image stamps (*HST* + *Spitzer*, ∼3.5 × 3.5 arcsec^2) of A370p_z1, showing a clear drop in $F105W$–$F814W$, typical of $z \gtrsim 6.5$ galaxies. The *Spitzer* channels have been decontaminated from the contribution of a southern object (see Section 3.1). *Lower panel*: Spectral energy distribution based on the photometry (black) with a BAGPIPES fit (red) adopting a redshift $z = 6.80$ from the Lyman α profile. Note a 3.6 μm excess likely due to [O III] + H β emission, claimed to be an indicator of high f_{esc}(LyC) (e.g. Faisst 2016; Izotov et al. 2018; Tang et al. 2019; Nakajima et al. 2020).

with evidence for strong [O II] and H β emission lines (Laporte et al. 2017b), we searched for similar sources using data from the *Hubble* and *Spitzer Space Telescopes* in the Frontier Fields survey (Lotz et al. 2017), applying selection criteria defined in Bouwens et al. (2015). Possible evidence for intense [O III] and H β line emission was considered via excess emission in the appropriate IRAC bandpasses (see Labbé et al. 2013; Smit et al. 2014).

Spectroscopic follow-up was conducted with both X-Shooter/VLT and ALMA (Laporte et al. 2017b, Hashimoto et al. 2018, Laporte et al. 2019) to determine the redshifts, star-formation rates (SFR) and other properties. Among this sample, one bright galaxy ($F125W = 25.16$, $z_{phot} = 7.14 \pm 0.8$), hereafter A370p_z1, was observed with X-Shooter/VLT in service mode in 2018 October. Observing blocks were defined in order to maximize the exposure time in the NIR arm ($t_{NIR} = 900$ s, $t_{Vis} = 819$ s, and $t_{UVB} = 756$ s). The target was centred in a 0.9 arcsec slit using a blind offset from a nearby bright star. After discarding time in poor seeing, the usable exposure time in the Vis arm was 6.3 h.

The spectroscopic data were reduced using standard X-Shooter ESOREFLEX recipes (v3.3.5). Flux calibrated 2D spectra were stacked using IRAF's *imcombine* and visually inspected for emission lines by two authors (RAM and NL). Stacking with custom ESOREFLEX and PYTHON recipes produced similar results. The stacked 2D spectrum was optimally extracted (Horne 1986) with a boxcar aperture of 1.6 arcsec (10 pixels) revealing an emission line doublet at 9484, 9487 Å (Fig. 1). No other line was found in the X-Shooter data.

The trough between the two peaks is about twice the X-Shooter resolution for the adopted 0.9 arcsec slit (34 km s^{-1}). To verify that the inter-peak absorption is significant, we compute the residuals of the dip pixels with respect to the flux of the smaller peak (the blue peak). The χ^2 statistic gives an only $P(\chi^2) = 0.00013$ probability that the dip is consistent with Gaussian residuals around the blue peak maximum. The inter-peak absorption is therefore significant at 3.8σ. However, this statistic does not guarantee that the double-peaked profile would be selected by eye when inspecting the 2D spectra. In order to recognize a double-peak, observers look for a few significantly absorbed pixels, preferably consecutive, in-between the peaks. We resampled the spectrum between $\lambda = 9480$, 9489 Å assuming a Gaussian noise distribution with variance drawn from the error array. We then identified the maximum pixels on either side of $\lambda = 9485$ Å to find the profile peaks. Counting how many pixels are >2σ below the average of the peaks' maximum flux, we found that in ∼ 95 per cent (2σ) of the resampled spectra, there are at least four pixels satisfying this criteria, and at least two are contiguous. We used this bootstrap resampling technique to obtain robust errors on the peak velocity separation $\Delta v = 101^{+38}_{-19}$ km s^{-1}. We note that these errors might be slightly underestimated because the peak separation is measured from the maximum of the peaks. A more conservative error estimate based on the resolution of the spectra (33.5 km s^{-1}) gives $\Delta v = 101 \pm 48$ km s^{-1}.

The observed peak separation rules out a $z \sim 1.54$ [O II] $\lambda\lambda$ 3727, 3729 interloper ($\Delta v = 225$ km s^{-1}) and a $z \sim 4.15$ C III]$\lambda\lambda$ 1907, 1909 doublet ($\Delta v = 314$ km s^{-1}). A low-redshift interpretation would predict other lines in the UV, Vis, and NIR arms but none was found (e.g. [O III] and [O II] are detectable with X-Shooter up to $z \sim 3.8$ and 5.4, respectively). A high-redshift solution is also consistent with the Lyman break seen in the SED (Fig. 2); a dusty source with a Balmer break at $z \sim 1.5-2$ is inconsistent with the flat SED redwards of 1.5 μm. Although it is possible the peaks come from different locations in a single galaxy or a merger, our 2D spectral data indicates both peaks are co-spatial.

We therefore conclude that A370p_z1 has a double-peaked Lyman α profile at $z = 6.803$ (taken as the mid-point of the two peaks[1])

[1] Verhamme et al. (2018) show that for all double-peaked profiles with known systemic redshift reported in the literature, the systemic redshift always falls

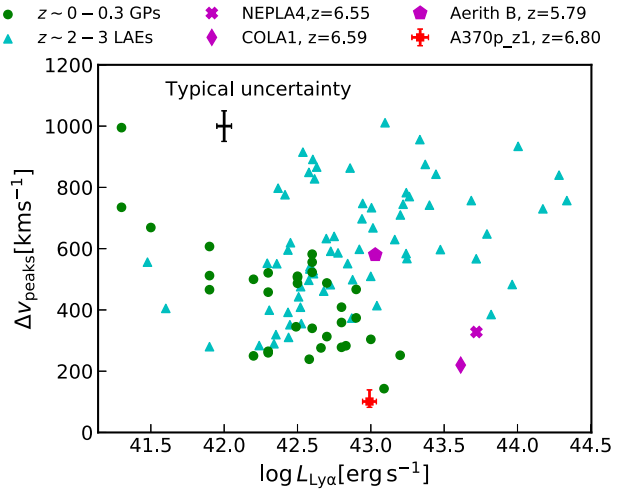

Figure 3. Lyman α peak separation versus Lyman α luminosities for $z \sim 0$ Green Peas (green circles; Yamada et al. 2012) and ∼2–3 double-peaked LAEs (cyan triangles; Kulas et al. 2012; Hashimoto et al. 2015; Yang et al. 2017), Aerith B (magenta pentagon; Bosman et al. 2020), NEPLA4 (magenta cross; Songaila et al. 2018), COLA1 (magenta diamond; Matthee et al. 2018), and A370p_z1 (red square).

with a peak velocity separation of $\Delta v = 101^{+38}_{-19}$ km s^{-1}. The Lyman α rest-frame luminosity ($(9.8 \pm 1.0) \times 10^{42}$ erg s^{-1}) and equivalent width ($EW_{Ly\alpha} = 43 \pm 4$ Å) are similar to those seen in $z \sim 0$ Green Peas (Yang et al. 2017; Izotov et al. 2018) or ∼2−3 double-peaked Lyman α emitters (LAEs, e.g. Kulas et al. 2012; Yamada et al. 2012; Hashimoto et al. 2015, see Fig. 3). Finally, Matthee et al. (2018) raised the possibility that high-redshift double-peaked Lyman α could be potentially caused by a foreground absorber in a standard (red-wing only) Lyman α line. However, the skewness of the red and (blue) peak is $S = 0.70 \pm 0.24$ (-0.32 ± 0.23) which is higher than the $S > 0.15$ threshold used for LAEs (Kashikawa et al. 2006). The skewness of the peaks also disfavours the merger interpretation. We searched for evidence of a hard ionization spectrum or AGN activity but, at the expected location of N IV 1240 Å, C IV 1549 Å, He II 1640 Å, C III]λλ1907, 1909 we do not find any significant emission lines (Fig. A1). Table 1 summarizes the properties of A370p_z1. The uncertainties are derived using the spectral resolution ($R \sim 8900$) and the error array, except for the peak velocity separation which comes from bootstrapping.

3 RESULTS

3.1 The nature of A370p_z1

We first characterized A370p_z1 by utilizing the available deep *HST* and *Spitzer* Frontier Fields imaging (Fig. 2, upper panel). We extracted the spectral energy distribution (SED) following the method described in Finkelstein et al. (2013). We neglect any lensing magnification as A370p_z1 is in a parallel field and thus far from the cluster Abell 370. The *Spitzer* 3.6 and 4.5 μm images are contaminated by a point source 1.5 arcsec to the south-east. We used GALFIT (Peng et al. 2010) to remove its contaminating contribution and applied a standard aperture correction. We fit the SED using

close to the mid-point of the peaks, in agreement with the findings of radiative-transfer simulations.

Table 1. Properties of A370p_z1. Limits are quoted at the 2σ level. The peak velocity separation and associated escape fraction are given with bootstrap errors and resolution errors (see Section 2).

RA	$02^h40^m14\overset{s}{.}1$
Dec.	$-01^d37^m14\overset{s}{.}3$
Emission lines	
$F_{Ly\alpha}$	$(18.4 \pm 1.9) \times 10^{-18}$ erg cm^{-2}s^{-1}
$F_{N\,V}$	$< 1.9 \times 10^{-18}$ erg cm^{-2}s^{-1}
$F_{C\,IV}$	$< 1.3 \times 10^{-18}$ erg cm^{-2}s^{-1}
$F_{He\,II}$	$< 2.6 \times 10^{-18}$ erg cm^{-2}s^{-1}
$F_{C\,III}$	$< 0.7 \times 10^{-18}$ erg cm^{-2}s^{-1}
Lyman α profile	
$z_{Ly\alpha}$	6.803
$\Delta v_{Ly\alpha}$	$101^{+38}_{-19}(\pm 48)$ km s^{-1}.
$FWHM_{blue}$	82 ± 48 km s^{-1}
$FWHM_{red}$	120 ± 48 km s^{-1}
f_{blue}	$(7.4 \pm 1.9) \times 10^{-18}$ erg cm^{-2}s^{-1}
f_{red}	$(10.8 \pm 2.4) \times 10^{-18}$ erg cm^{-2}s^{-1}
Blue/red flux ratio	0.69 ± 0.24
Blue peak skewness	-0.32 ± 0.23
Red peak skewness	0.70 ± 0.24
$L_{Ly\alpha}$ (rest-frame)	$(9.8 \pm 1.0) \times 10^{42}$erg s^{-1}
$EW_{Ly\alpha}$ (rest-frame)	43 ± 4 Å
f_{esc}(LyC) (Izotov et al. 2018)	>0.59(>0.51)
f_{esc}(LyC) (RASCAS)	0.99
Photometry and SED fitting (BAGPIPES)	
m_{F435W}	<29.90
m_{F606W}	<29.80
m_{F814W}	<30.00
m_{F105W}	25.41 ± 0.01
m_{F125W}	25.16 ± 0.01
m_{F140W}	25.17 ± 0.01
m_{F160W}	25.16 ± 0.01
$m_{3.6\mu}$	24.85 ± 0.14
$m_{4.5\mu}$	26.19 ± 0.50
$M_{UV}(m_{F105W})$	-21.5 ± 0.1
M_*	$(6.55^{+0.14}_{-0.10}) \times 10^9$ M$_\odot$
SFR	12 ± 6 M$_\odot$ yr^{-1}
Age	50 ± 4 Myr

BAGPIPES (Carnall et al. 2018), experimenting with several star formation histories (SFH) adopting single (constant, exponential, burst) and two-component models (constant + burst ; exponential + burst). The best-fitting SED was a constant SFH model with the following properties: age $= (50 \pm 4)$ Myr, $M_\star = (6.55^{+0.14}_{-0.10}) \times 10^9$ M$_\odot$, and an SFR $= (12 \pm 6)$ M$_\odot$yr^{-1} (Fig. 2, lower panel, and Table 1). We found no preference for an exponentially declining SFH or a single-burst model. The flux limits at the rest-frame UV lines positions are consistent with the line fluxes from the best-fitting SED (see further Table 1).

As discussed in Section 1, a small separation for a double-peaked Lyman α profile is a strong indicator of a high LyC escape fraction in low-redshift analogues (e.g. Gronke 2017; Verhamme et al. 2017). However, the tight empirical relation found by Izotov et al. (2018),

$$f_{esc}(\mathrm{LyC}) = \frac{3.23 \times 10^4}{\Delta v^2_{Ly\alpha}} + \frac{1.05 \times 10^2}{\Delta v_{Ly\alpha}} + 0.095\,, \quad (1)$$

may not apply for the range $v_{peaks} \lesssim 150$ km s^{-1} which was not probed by their observations and where their relation would predict an unphysical f_{esc}(LyC) > 100 per cent. We therefore put a maximum of 100 per cent to the polynomial function so it does not result in unphysical values. We then compute the escape fraction for

Table 2. Shell model parameter grid searched.

b (km s^{-1})	20, 80, 140
$v_{\rm exp}$ (km s^{-1})	0, 20, 50
log $N_{\rm H\,I}$ (cm^{-2})	15, 16, 17, 18
$\tau_{\rm d}$	0, 0.5, 1
FWHM$_{{\rm Ly}\alpha}$ (km s^{-1})	100, 200, 300, 400, 500

each of the resampled spectra (see Section 2) to obtain a 2σ lower limit on A370p_z1 LyC escape fraction $f_{\rm esc}$(LyC) > 59 per cent. Using the conservative error from the X-Shooter resolution gives $f_{\rm esc}$(LyC) > 51 per cent (2σ).

In order to better estimate the escape fraction, we compare the observed profile with double-peak shell models. We use the RASCAS 3D Monte Carlo code (Michel-Dansac et al. 2020) to generate a grid of Lyman α radiation transfer simulations in spherical geometries, allowing for static and expanding gas configurations. In these typical shell models (e.g. Dijkstra, Haiman & Spaans 2006; Verhamme et al. 2008), H I gas and dust are distributed homogeneously around a central point source. The shell is described by four physical parameters, namely the expanding velocity $v_{\rm exp}$, the H I column density $N_{\rm H\,I}$, the dust opacity $\tau_{\rm d}$, and the Doppler parameter b which accounts for the thermal/turbulent gas motions (see Table 2 for the parameter grid used). The intrinsic emission is assumed to be a Gaussian line centred on the systemic redshift with a width set by the FWHM. Given the nearly symmetric double-peaked profile of A370p_z1 and the small peak separation, we restrict our analysis to relatively small $N_{\rm H\,I}$ and $v_{\rm exp}$ values because it is well known that high column densities and shell velocities would significantly broaden the line and erase the blue peak, respectively (Verhamme, Schaerer & Maselli 2006). We perform a quantitative comparison between the observed line profile and the models using the χ^2 statistic. We find that models minimizing the reduced χ^2 preferentially select low $N_{\rm H\,I}$ (log $N_{\rm H\,I}$/[cm^{-2}] = 15), static geometries ($v_{\rm exp}$ = 0), low dust content, small b values (b = 20) and relatively broad input lines (200 km s^{-1} < FWHM$_{{\rm Ly}\alpha}$ < 400 km s^{-1}).

We show the best-fitting model in Fig. 4 which corresponds to the following parameter set: log $N_{\rm H\,I}$/[cm^{-2}] = 15, b = 20 km s^{-1}, $v_{\rm exp}$ = 0, FWHM = 300 km s^{-1}. We can derive the LyC escape fraction from the best-fitting column density $f_{\rm esc}$(LyC) = exp ($-\sigma_{912}N_{\rm H\,I}$) = 99 per cent, where $\sigma_{912} = 6.35 \times 10^{-18}$ is the H I photoionization cross-section at the Lyman limit. While several models could match the positions of peak emission within the errors, the log $N_{\rm H\,I}$/[cm^{-2}] = 10^{15} model is the only one to reproduce the shallow central depression of the profile which is the important signature of a low H I opacity (Fig. 4). Searching a finer parameter grid is beyond the scope of this paper, but we note that even when adopting a higher column density log $N_{\rm H\,I} = 10^{16}$ cm^{-2}, the escape fraction remains very high (94 per cent).

3.2 Did A370p_z1 self-ionize its local H II bubble?

The detection of the blue peak in the Lyman α indicates A370p_z1 sits in a large ionized bubble, otherwise the damping wing of even a partially neutral IGM would have absorbed it. Given its high escape fraction, we now consider whether A370p_z1 could have self-ionized its local H II bubble.

The blue wing extends to λ = 9479.2 Å, $\approx$ 215 km s^{-1} from the line centre, corresponding to a physical distance $r_{\rm H\,II} > 0.26 \pm 0.04$ pMpc. This estimate neglects any velocity offset between the Lyman α absorption dip from which we have derived the redshift and the systemic redshift as defined by more reliable tracers such as

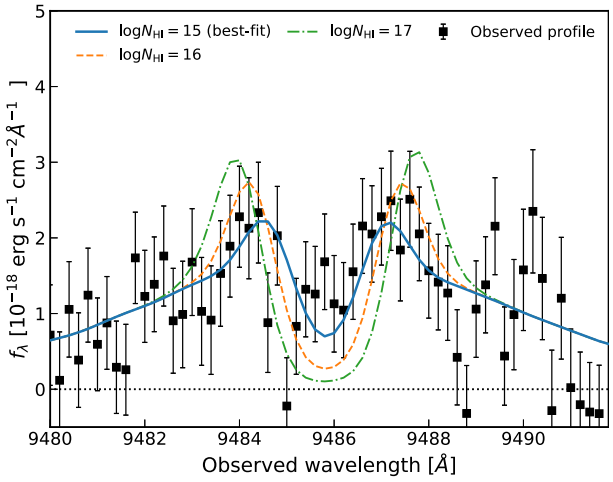

Figure 4. Comparison of RASCAS models, smoothed by the resolution of X-Shooter, of Lyman α transfer through non-expanding shells of homogeneous gas with the observed Lyman α profile. The best-fitting model (blue) has log $N_{\rm H\,I}$/[cm^{-2}] = 10^{15} which correspond to a high LyC escape fractions $f_{\rm esc}$(LyC) = 99 per cent. We also show examples of models with log $N_{\rm H\,I}$/[cm^{-2}] = 10^{16}(10^{17}) (dashed orange, dash–dotted green), which would imply $f_{\rm esc}$(LyC) = 94 per cent(53 per cent).

nebular absorption lines. These velocities are however found to be $\lesssim$ 200 km s^{-1} (Gazagnes et al. 2020), which, in the worst case, would therefore require a larger ionized bubble for the blue wing to be transmitted ($\lesssim$ 0.5 pMpc). We also neglect peculiar velocities of the galaxy with respect to the ionized bubble gas which would redshift(blueshift) the Lyman α photons and decrease(increase) the bubble size needed for the blue wing to escape.

We now estimate the volume that could have been reionized by A370p_z1 by redshift z = 6.803 and whether its radiation is sufficient to reduce the opacity of the surrounding gas to permit the blue wing of Lyman α to escape. Assuming no recombination, the ionized bubble (Strömgren sphere) created by a single galaxy in the reionization era is (e.g. Cen & Haiman 2000)

$$R_{\rm S} \approx \left(\frac{3 f_{\rm esc}({\rm LyC}) \xi_{\rm ion,LyC} L_{\rm UV} t_{\rm em}}{4\pi \langle n_{\rm H\,I} \rangle} \right)^{1/3}, \quad (2)$$

where $t_{\rm em}$ is the duration of LyC leakage from a source with intrinsic ionizing efficiency $\xi_{\rm ion,LyC}$ and escape fraction $f_{\rm esc}$(LyC) and $\langle n_{\rm H\,I}(z) \rangle \approx 8.5 \times 10^{-5} \left(\frac{1+z}{8}\right)^3$ cm^{-3} is the mean hydrogen density of the IGM. The typical ionizing efficiency of $M_{\rm UV} = -22$ galaxies at $z \sim 5$ is log $\xi_{\rm ion} \simeq$ 25.4 cgs (Bouwens et al. 2015). However, recently it has been claimed that some $z > 7$ galaxies have enhanced ionizing efficiencies (Stark et al. 2015, 2017). We therefore derive an estimate of the ionizing efficiency from the Lyman α line following Sobral & Matthee (2019) and find log $\xi_{\rm ion} \simeq$ 26.4 cgs.[2] In the following, we indicate results based on the higher ionizing

[2]As cautioned by Sobral & Matthee (2019), this low-redshift estimator of the LyC photon production rate might not apply to high-redshift LAEs. In particular, it relies on a linear relationship between the Lyman-alpha escape fraction and equivalent width which implies an escape fraction of Lyman-alpha photons of ∼20% for A370p_z1, in contradiction with our LyC escape fraction measurement. We keep this enhanced ionising efficiency value for A370p_z1 throughout the discussion for a fairer comparison with NEPLA4 and COLA1 in Section 4. We note that the value of 26.4 cgs is similar to the ionising efficiencies reported in other high-redshift objects (Stark et al. 2015, 2017).

efficiency in parenthesis. Assuming an $f_{\rm esc}({\rm LyC}) \approx 0.9$, 50 Myr is a sufficient time for A370p_z1 to create an ionized bubble with radius $R_{\rm S} \simeq 0.86(1.10)$ pMpc. This is more than three times larger than the distance at which the blue wing of Lyman α is still transmitted. Therefore, it is plausible that A370p_z1 is able to self-ionize its surrounding bubble, even if the escape fraction was ≈ 90 per cent only for a small fraction of its lifetime (e.g. $R_{\rm S}(t_{\rm em} = 0.2t_{\rm age}) \approx 0.50(1.05)$ pMpc).

Being able to grow a Strömgren sphere larger than the distance required for the blue wing of Lyman α to redshift out of resonance is a necessary but not sufficient condition for A370p_z1 to be solely responsible for its ionized bubble. This is because the Gunn–Peterson optical depth is virtually zero for neutral fractions as low as $10^{-4.5}$ (see Becker, Bolton & Lidz 2015a, for a review). Therefore, in the absence of an elevated photoionization rate, the blue peak would readily be resonantly absorbed by even small pockets of neutral gas within the ionized bubble. We therefore examine whether A370p_z1 can maintain such a high photoionization rate at the edge of its bubble or if an additional population of clustered UV-faint galaxies is required.

Following Kakiichi et al. (2018, and references therein), the local photoionization rate due to A370p_z1 is

$$\Gamma_{\rm H\,I}^{\rm A370p\_z1}(r) = \frac{\alpha_{\rm g}\sigma_{912}}{\alpha_{\rm g}+3}\frac{f_{\rm esc}({\rm LyC})\xi_{\rm ion}L_{\rm UV}}{4\pi r^2}{\rm e}^{-{\rm r}/\lambda_{\rm mfp}} \simeq 0.8(7.4)\times10^{-11}\left(\frac{r}{0.1\,{\rm pMpc}}\right)^{-2}{\rm s}^{-1}, \quad (3)$$

where $\alpha_{\rm g}$ is the extreme UV spectral slope and $\lambda_{\rm mfp}$ is the mean free path of LyC photons. We assume $\alpha_{\rm g} = 2$ (e.g. Kuhlen & Faucher-Giguère 2012) and $\lambda_{\rm mfp} \simeq 6.0\left(\frac{1+z}{7}\right)^{-5.4}$ pMpc (Worseck et al. 2014). The fluctuating Gunn–Peterson approximation links the photoionization rate Γ to the Lyman α opacity $\tau_\alpha \simeq 11\Delta_b^{2-0.72(\gamma-1)}\left(\frac{\Gamma_{\rm H\,I}}{10^{-12}\,{\rm s}^{-1}}\right)^{-1}\left(\frac{T_0}{10^4\,{\rm K}}\right)^{-0.72}\left(\frac{1+z}{7}\right)^{9/2}$ (see Becker et al. 2015a, for a review), where Δ_b is the baryon overdensity and the temperature T_0 is assumed to be 10^4 K.

At a constant mean density of $\Delta_b = 1$, the photoionization rate due to A370p_z1 is sufficient to have an average Lyman α transmission in the bubble $\overline{\mathcal{T}_\alpha}({\rm blue\ wing}) = 0.25(0.69)$, and a transmission at the edge of the blue peak $\mathcal{T}_\alpha^{\rm blue\,peak} = 0.51(0.93)$. We note this does not take into account expansion in the Hubble flow, ignores the effect of the IGM damping wing or overdensities associated with the galaxy, enhancements we consider beyond the scope of this discovery paper. Recently, Mason & Gronke (2020) have laid out an extensive framework to model high-redshift double-peaked Lyman α emitters. Their modelling suggests that a source with the luminosity of A370p_z1 and $f_{\rm esc}({\rm LyC}) = 1$ could carve an ionized bubble with $r_{\rm ion} \sim 0.6$ pMpc sufficient to permit the blue peak to escape up to $\sim$0.2 pMpc, in good agreement with our results.

Finally, we checked that A370p_z1 does not lie in an overdensity of $z \sim 6.8$ objects. We find 28 $F105W$–$F814W$ dropout galaxies in the A370p field with $M_{F125W} < 28$ whose 1σ photometric redshift is at least partially in the redshift interval $6.3 < z < 7.3$. This is in good agreement to that expected (28 ± 5) from the Bouwens et al. (2015) UV luminosity function. We thus conclude that A370p_z1 is very likely to have contributed to the totality or the large majority of the LyC photons in its surrounding ionized bubble.

Table 3. Comparison of the ionizing properties of the three known $z \sim 6.5$ double peaks. Strömgren radii are computed assuming ages of 10 Myr.

	NEPLA4	COLA1	A370p_z1
$M_{\rm UV}$	-21.8	-21.6	-21.5
$f_{\rm esc}({\rm LyC})(\Delta{\rm v})$	0.11	0.29	$\approx$0.9
${\rm EW_{Ly\alpha}}$ (Å)	176	120	43
r_α (pMpc)	0.31	0.31	0.26
Assuming $\xi_{\rm ion,LyC} = 10^{25.4}$ cgs			
$r_{\rm S}$ (pMpc)	0.29	0.37	0.50
$\langle T_\alpha\rangle$(blue wing)	0.09	0.13	0.25
T_α(blue peak)	1×10^{-16}	7×10^{-5}	0.51
Deriving $\xi_{\rm ion,LyC}$ from Lyman α (Sobral & Matthee 2019)			
$\xi_{\rm ion,LyC}$	$10^{25.38}$	$10^{25.66}$	$10^{26.38}$
$r_{\rm S}$ (pMpc)	0.28	0.45	1.05
$\langle T_\alpha\rangle$(blue wing)	0.09	0.17	0.69
T_α(blue peak)	3×10^{-17}	6×10^{-3}	0.93
Peak flux ratio	$\approx$0.6	0.31 ± 0.03	0.93 ± 0.28

4 DISCUSSION

4.1 Differences and similarities between NEPLA4, COLA1, and A370p_z1

We now apply the methodology described in the previous section to determine which $z > 6$ double-peaks (A370p_z1, COLA1, and NEPLA4) can grow an H II bubble and ionize it sufficiently to permit blue peak photons to escape. We leave Aerith B aside as the ionized bubble created by the nearby quasar was studied in detail by Bosman et al. (2020). For this exercise, we assume that the redshift of all three objects is taken from the mid-point of the two Lyman α peaks. To further facilitate the comparison between objects, we assume an age of 10 Myr for each galaxy (which matches the estimate for COLA1 in Matthee et al. (2018), but is lower than what we measure for A370p_z1). This only affects the Strömgren bubble radii which are proportional to $\propto t_{\rm em}^{1/3}$ and can be rescaled accordingly if needed. The escape fractions, UV magnitudes, and extent of the blue wings r_α presented in Table 3 are taken from Matthee et al. (2018), Songaila et al. (2018), and Songaila (private communication).

Interestingly, we find that all double-peaks can grow a Strömgren sphere as large as the minimum bubble size r_α derived from the blue wing maximum velocity offset. However, only A370p_z1 can grow a bubble that is 2–4 times larger (depending on the ionizing efficiency). This is important because the calculated radius of the Strömgren sphere is significantly larger than the maximum distance at which blue photons still escape (Mason & Gronke 2020). The most significant test of whether a galaxy is self-ionizing its local bubble, or if additional faint sources are needed to let the blue wing photons escape, is to compute the opacity to Lyman α photons. We find that COLA1 and NEPLA4 are unable to solely ionized the CGM/IGM sufficiently to allow blue peak photons to escape. The predicted opacity at the blue peak is 0.6 per cent in the most favourable scenario for COLA1, and always zero for NEPLA4. However, the blue peaks are clearly detected, with an observed blue/red peak flux ratio of 0.31 for COLA1 and 0.6 for NEPLA4. We conclude that additional sources are needed to maintain their H II bubbles highly ionized. In contrast, A370p_z1 is able to maintain its bubble sufficiently ionized on its own in all scenarios within the large 1σ error of the peak flux ratio. Collectively, the four currently known high-redshifts double-peaks present a large range of cases from a source not contributing to reionization (Aerith B) to a powerful source ionizing its H II bubble (A370p_z1), and intermediate cases with significant $f_{\rm esc}$(LyC) but

probably surrounded with faint leakers which keep their H II bubble highly ionized (NEPLA4, COLA1).

4.2 Implications for reionization

We have shown that A370p_z1 is possibly the first convincing example of a source capable, *on its own*, of creating a significant ionized bubble *and* maintaining this state so that photons escape bluewards of Lyman α. A key question therefore is whether it is an exceptional source or representative of a larger population of luminous objects responsible for concluding cosmic reionization. Although many luminous $z > 6$ galaxies have now been spectroscopically confirmed using the Lyman α line (e.g. Zitrin et al. 2015; Laporte et al. 2017a, b; Stark et al. 2017; Hashimoto et al. 2018; Songaila et al. 2018; Stark et al. 2018; Taylor et al. 2020), the majority did not have the spectral resolution to resolve closely separated peaks as is the case in A370p_z1. Additionally, very shallow blue peaks below the sensitivity limit of the observations would also be missed. None the less, the unusually high confirmation rate of Lyman α emission in the Roberts-Borsani et al. (2016) galaxies with strong IRAC 4.5 μm excesses might be explained if they were efficient leakers that carved their own ionized bubbles (Zitrin et al. 2015; Stark et al. 2017). Alternatively, of course, there may be associated faint sources and/or AGN activity that contribute to the ionizing flux.

Searching for a larger sample of $z > 6$ double-peaked Lyman α emitters is therefore a promising way of studying both the sources of reionization and their surrounding H II bubbles with the growing modelling capabilities highlighted above. The rest-frame optical lines of these luminous $z > 6$ sources will be detectable with *JWST*, enabling us to characterize, amongst other quantities, their intrinsic ionizing output.

ACKNOWLEDGEMENTS

We wish to thank the anonymous referee for comments which significantly improved this manuscript. RAM, NL, RSE acknowledge funding from the European Research Council (ERC) under the European Union's Horizon 2020 research and innovation programme (grant agreement no. 669253). NL also acknowledges support from the Kavli Foundation. AV acknowledges support from the SNF under the professorship grant 176808. AV and TG acknowledge support from the European Research Council under grant agreement ERC-stg-757258 (TRIPLE). RAM thanks K. Kakiichi, M. Gronke, and J. Matthee for useful discussions. We are grateful to A. Songaila for sharing details about the blue wing of NEPLA4 and its *Y*-band magnitude. This study is based on observations made with ESO Telescopes at the La Silla Paranal Observatory under programme 0100.A-0664(A).

DATA AVAILABILITY

The data underlying this article are available in the ESO archive (archive.eso.org) under programme ID 0100.A-0664(A).

REFERENCES

Bañados E. et al., 2019, ApJ, 885, 59
Bassett R. et al., 2019, MNRAS, 483, 5223
Becker G. D., Bolton J. S., Lidz A., 2015a, Publ. Astron. Soc. Aust., 32, e045
Becker G. D., Bolton J. S., Madau P., Pettini M., Ryan-Weber E. V., Venemans B. P., 2015b, MNRAS, 447, 3402
Bosman S. E. I., Kakiichi K., Meyer R. A., Gronke M., Laporte N., Ellis R. S., 2020, ApJ, 896, 49
Bouwens R. J. et al., 2015, ApJ, 803, 34
Carnall A. C., McLure R. J., Dunlop J. S., Davé R., 2018, MNRAS, 480, 4379
Cen R., Haiman Z., 2000, ApJ, 542, L75
Dayal P., Ferrara A., 2018, Phys. Rep., 780–782, 1
Dayal P. et al., 2020, MNRAS, 495, 3065
Dijkstra M., 2014, Publ. Astron. Soc. Aust., 31, E040
Dijkstra M., Haiman Z., Spaans M., 2006, ApJ, 649, 14
Faisst A. L., 2016, ApJ, 829, 99
Finkelstein S. L. et al., 2013, Nature, 502, 524
Finkelstein S. L. et al., 2019, ApJ, 879, 36
Fletcher T. J., Tang M., Robertson B. E., Nakajima K., Ellis R. S., Stark D. P., Inoue A., 2019, ApJ, 878, 87
Gazagnes S., Chisholm J., Schaerer D., Verhamme A., Izotov Y., 2020, A&A, 639, A85
Gronke M., 2017, A&A, 608, A139
Hashimoto T. et al., 2015, ApJ, 812, 157
Hashimoto T. et al., 2018, Nature, 557, 392
Horne K., 1986, PASP, 98, 609
Hu E. M., Cowie L. L., Songaila A., Barger A. J., Rosenwasser B., Wold I. G. B., 2016, ApJ, 825, L7
Izotov Y. I., Worseck G., Schaerer D., Guseva N. G., Thuan T. X., Fricke Verhamme A., Orlitová I., 2018, MNRAS, 478, 4851
Kakiichi K., Gronke M., 2019, preprint (arXiv:1905.02480)
Kakiichi K. et al., 2018, MNRAS, 479, 43
Kashikawa N. et al., 2006, ApJ, 648, 7
Kuhlen M., Faucher-Giguère C.-A., 2012, MNRAS, 423, 862
Kulas K. R., Shapley A. E., Kollmeier J. A., Zheng Z., Steidel C. C., Hainline K. N., 2012, ApJ, 745, 33
Labbé I. et al., 2013, ApJ, 777, L19
Laporte N. et al., 2017a, ApJ, 837, L21
Laporte N., Nakajima K., Ellis R. S., Zitrin A., Stark D. P., Mainali R., Roberts-Borsani G. W., 2017b, ApJ, 851, 40
Laporte N. et al., 2019, MNRAS, 487, L81
Lotz J. M. et al., 2017, ApJ, 837, 97
Mason C. A., Gronke M., 2020, MNRAS, 449, 1395
Matthee J., Sobral D., Gronke M., Paulino-Afonso A., Stefanon M., Röttgering H., 2018, A&A, 619, A136
Michel-Dansac L., Blaizot J., Garel T., Verhamme A., Kimm T., Trebitsch M., 2020, A&A, 635, A154
Naidu R. P., Tacchella S., Mason C. A., Bose S., Oesch P. A., Conroy C., 2020, ApJ, 892, 109
Nakajima K., Fletcher T., Ellis R. S., Robertson B. E., Iwata I., 2018, MNRAS, 477, 2098
Nakajima K., Ellis R. S., Robertson B. E., Tang M., Stark D. P., 2020, ApJ, 889, 161
Oke J. B., 1974, ApJS, 27, 21
Peng C. Y., Ho L. C., Impey C. D., Rix H. W., 2010, AJ, 139, 2097
Planck Collaboration VI, 2018, A&A, 641, A6
Roberts-Borsani G. W. et al., 2016, ApJ, 823, 143
Robertson B. E., Ellis R. S., Furlanetto S. R., Dunlop J. S., 2015, ApJ, 802, L19
Smit R. et al., 2014, ApJ, 784, 58
Sobral D., Matthee J., 2019, A&A, 623, A157
Songaila A., Hu E. M., Barger A. J., Cowie L. L., Hasinger G., Rosenwasser B., Waters C., 2018, ApJ, 859, 91
Stark D. P., Ellis R. S., Chiu K., Ouchi M., Bunker A., 2010, MNRAS, 408, 1628
Stark D. P. et al., 2015, MNRAS, 454, 1393
Stark D. P. et al., 2017, MNRAS, 464, 469
Stark D. P. et al., 2018, MNRAS, 477, 2513
Tang M., Stark D. P., Chevallard J., Charlot S., 2019, MNRAS, 489, 2572
Taylor A. J., Barger A. J., Cowie L. L., Hu E. M., Songaila A., 2020, ApJ, 895, 132
Verhamme A., Schaerer D., Maselli A., 2006, A&A, 460, 397
Verhamme A., Schaerer D., Atek H., Tapken C., 2008, A&A, 491, 89

Verhamme A., Orlitová I., Schaerer D., Hayes M., 2015, A&A, 578, A7
Verhamme A., Orlitová I., Schaerer D., Izotov Y., Worseck G., Thuan T. X., Guseva N., 2017, A&A, 597, A13
Verhamme A. et al., 2018, MNRAS, 478, L60
Worseck G. et al., 2014, MNRAS, 445, 1745
Yamada T., Matsuda Y., Kousai K., Hayashino T., Morimoto N., Umemura M., 2012, ApJ, 751, 29
Yang H. et al., 2017, ApJ, 844, 171
Zitrin A. et al., 2015, ApJ, 810, L12

APPENDIX A: NON-DETECTIONS OF REST-FRAME UV LINES

We show in Fig. A1 the 1D and 2D spectrum of A370p_z1 at the expected location of rest-frame UV lines. We do not find any significant lines (see Table 1 for detection limits).

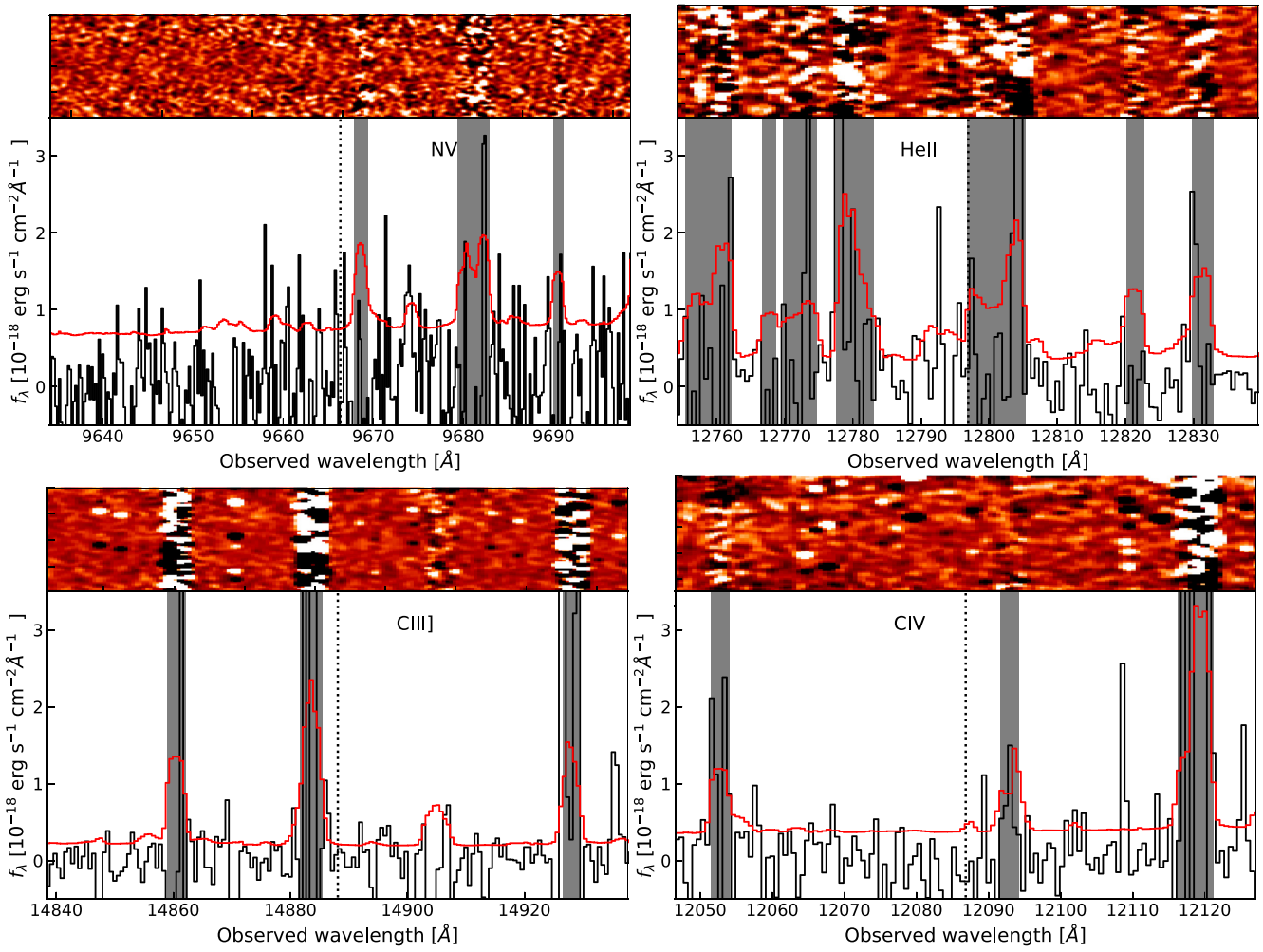

Figure A1. 2D and 1D spectrum of A370p_z1, showing the expected location of rest-frame UV lines at $z = 6.803$ (x-axis range: $\pm 1000\,\mathrm{km\,s^{-1}}$). Real emission lines should show one bright line at the centre of the 2D spectra (upper panel) with two negative counterparts (black) at the top and bottom of the spectrum due to the ABBA nodding pattern adopted. The colour scheme is identical to that of Fig. 1, but the smoothing length is adjusted for the NIR arm. The lower panel shows the 1D spectrum (black) and error array (red) with sky lines masked in grey. Vertical dotted lines show the exact wavelength of the UV lines or the centroid for doublets.

This paper has been typeset from a TEX/LATEX file prepared by the author.